Hybrid simulations of magnetic reconnection with kinetic ions and fluid electron pressure anisotropy

Le, Ari Yitzchak
Daughton, William Scott
Karimabadi, Homa
Egedal, Jan

To be published in: Physics of Plasmas

DOI to publisher's version: 10.1063/1.4943893

Hybrid Simulations of Magnetic Reconnection with Kinetic Ions and Fluid Electron Pressure Anisotropy

A. Le,[1] W. Daughton,[1] H. Karimabadi,[2] and J. Egedal[3]

[1] *Los Alamos National Laboratory, Los Alamos, New Mexico 87545, USA*

[2] *University of California—San Diego, La Jolla, California 92093 USA*

[3] *University of Wisconsin—Madison, Madison, Wisconsin 53706, USA*

Abstract

We present the first hybrid simulations with kinetic ions and recently developed equations of state for the electron fluid appropriate for reconnection with a guide field. The equations of state account for the main anisotropy of the electron pressure tensor. Magnetic reconnection is studied in two systems, an initially force-free current sheet and a Harris sheet. The hybrid model with the equations of state is compared to two other models, hybrid simulations with isothermal electrons and fully kinetic simulations. Including the anisotropic equations of state in the hybrid model provides a better match to the fully kinetic model. In agreement with fully kinetic results, the main feature captured is the formation of an electron current sheet that extends several ion inertial lengths. This electron current sheet modifies the Hall magnetic field structure near the X-line, and it is not observed in the standard hybrid model with isotropic electrons. The saturated reconnection rate in this regime nevertheless remains similar in all three models. Implications for global modeling are discussed.

I. INTRODUCTION

Magnetic reconnection plays a central part in the dynamics of the magnetosphere, the solar wind, the solar corona, and a variety of other space plasmas where particle collisions are negligible [1]. In these collisionless plasmas, kinetic effects may strongly modify the evolution of reconnecting current sheets. Observing the small-scale layers, typically referred to as diffusion regions, where kinetic effects are essential is a main goal of NASA's MMS mission [2]. As higher-resolution observations become available, it is more important to accurately reproduce the fine details of the reconnection layers when comparing numerical simulations to measurements.

Resolving all of the kinetic scales in simulations of very large systems or in global models is generally not feasible. For this reason, a variety of reduced models have been considered for simulating magnetic reconnection [3]. While the Hall MHD model was found to be a minimal model that allows reconnection to proceed at a fast rate comparable to observations, Hall MHD does not reproduce the details of the reconnection region. One proposal to capture these details is to use higher-order fluid moment equations that retain pressure anisotropy, pressure agyrotropy, and thermal heat fluxes [4–7]. In general, however, it remains unclear how to correctly truncate the fluid hierarchy of equations for collisionless systems, and these simulations typically rely on tuned transport parameters to match fully kinetic simulations.

Another approach is to only retain the ion kinetic effects. Hybrid modeling, in which the ions are treated kinetically and the electrons are treated as a fluid, offers a means of studying the ion kinetics of reconnection [8–10] without resolving the electron kinetic scales. A number of hybrid codes have been used to study ion kinetic effects in magnetic reconnection, some including ad hoc treatments of the electron pressure tensor [11–19]. The importance of treating the ions kinetically was demonstrated in a recent comparison of fluid, hybrid, and fully kinetic models of magnetic island merging, where reconnection was found to be qualitatively different between kinetic and fluid ion models even on MHD scales [20].

In hybrid codes, the question remains of what closure to employ for the electron fluid. Anisotropic equations of state for the main components of the electron pressure tensor, $p_{e\|}$ along the local magnetic field and $p_{e\perp}$ perpendicular to the field, have been derived for conditions typical of reconnection with a guide magnetic field [21]. A primary mechanism for generating the electron pressure anisotropy is the adiabatic trapping of electrons in a parallel electric field structure [22, 23]. While this anisotropy is not capable of breaking the frozen flux condition in itself [24], the electron pressure anisotropy strongly modifies the structure of the current layers that develop in the reconnection layer [25–28]. Depending on the strength of the guide magnetic field and the electron β_e, several different regimes are possible for the reconnection region [26]. The anisotropy is especially important in a regime with a range of intermediate guide magnetic fields, where the electron anistropy with $p_{e\|} > p_{e\perp}$ drives a current sheet that extends several d_i from the X-line and is not limited to electron kinetic scales. This regime has so far only been produced in fully kinetic simulations with high mass ratios $m_i/m_e \gtrsim 400$ [26], and it is therefore not yet possible to study this regime in large 3D systems with a fully kinetic treatment.

Here, we implement the anisotropic electron equations of state in the hybrid code H3D [17] and simulate the reconnection of a force-free current sheet and a Harris sheet, both including a guide magnetic field. While the reconnection of a force-free sheet has previously been studied in a two-fluid framework including the electron equations of state [25], the simulations presented are the first to additionally include ion kinetics. Simulating the reconnection of a Harris sheet with the electron equations of state entails additional complications, and such simulations have not previously been performed. In each case, the hybrid model including electron anisotropy reproduces details of the reconnection region observed in fully kinetic simulations. In particular, extended electron current sheets develop in the exhaust in the hybrid model with electron anisotropy that are comparable to the fully kinetic results, while the current layer remains short in the the hybrid model with isotropic electrons. The current sheet modifies the structure of the Hall magnetic fields, while the the saturated reconnection rate remains similar in both hybrid models and the fully kinetic model.

II. HYBRID MODEL AND EQUATIONS OF STATE

In the hybrid code H3D [17], ions are treated kinetically by the particle-in-cell method. The electrons are treated as a massless fluid, and the electron dynamics enter through an Ohm's law for the electric field of the form:

$$\mathbf{E} = -\mathbf{u_i} \times \mathbf{B} + \frac{1}{ne}\mathbf{J} \times \mathbf{B} - \frac{1}{ne}\nabla \cdot \mathbb{P}_e + \eta\mathbf{J} - \eta_H \nabla^2 \mathbf{J} \quad (1)$$

where the current density is defined through Ampere's law without displacement current $\mu_0 \mathbf{J} = \nabla \times \mathbf{B}$ (implying the system is non-relativistic and does not resolve light waves). The magnetic field is evolved as usual with Faraday's law $\partial \mathbf{B}/\partial t = -\nabla \times \mathbf{E}$.

The equations are completed by a fluid closure for the electron pressure tensor $\mathbb{P}_e$. The simplest closure is found by assuming an isotropic pressure p_e with an equation of state of the form $p_e \propto n^\gamma$, where quasi-neutrality is assumed and the electron density n is therefore set equal to the ion density computed from the numerical ions within each cell of the computational grid. A value of $\gamma = 1$ gives the isothermal limit, and $\gamma = 5/3$ is the adiabatic limit.

Anisotropy of the electron pressure tensor, however, has been found to dominate the dynamics of the diffusion region where electron current layers form [27], pointing to the need to capture this effect in the electron fluid closure. A primary mechanism for generating the electron pressure anisotropy is the adiabatic trapping of electrons in a parallel electric field structure [21–23, 29]. This mechanism follows from a drift kinetic treatment with the additional assumption that the parallel motion of trapped electons is adiabatic. It therefore applies to general geometries with expanding or contracting flux tubes, and it is not limited to the reconnection problem. For the case of reconnection, the electron trapping produces electron pressure anisotropy with components $p_{e\parallel}$ along the local magnetic field and $p_{e\perp}$ perpendicular such that typically $p_{e\parallel} > p_{e\perp}$ in the reconnection layer.

When a given magnetic flux tube extends into an upstream region with uniform plasma conditions, the equations of state depend only on the local values of the density n and magnetic field strength B normalized to their upstream values in the flux tube. For upstream plasma that contains isotropic Maxwellian electrons at density n_∞, pressure p_∞, and an ambient magnetic field of strength B_∞, the equations of state take the approximate form [21]:

$$\tilde{p}_{e\parallel}(\tilde{n}, \tilde{B}) = \tilde{n}\frac{2}{2+\alpha} + \frac{\pi \tilde{n}^3}{6\tilde{B}^2}\frac{2\alpha}{2\alpha+1} \tag{2}$$

$$\tilde{p}_{e\perp}(\tilde{n}, \tilde{B}) = \tilde{n}\frac{1}{1+\alpha} + \tilde{n}\tilde{B}\frac{\alpha}{\alpha+1} \tag{3}$$

where $\alpha = \tilde{n}^3/\tilde{B}^2$ and, for any quantity Q, $\tilde{Q} = Q/Q_\infty$. These are the equations of state implemented in our hybrid code to account for electron pressure anisotropy. The expressions in Eqs. 2 and 3 above highlight two opposite limits. For $\alpha \ll 1$, there are essentially no trapped electrons, and the equations of state reduce to the isothermal form $p_{e\parallel} = p_{e\perp} = nT_\infty$

with a uniform temperature. In the opposite limit of $\alpha \gg 1$, most electrons are trapped and cannot carry a heat flux, so the electrons follow the double adiabatic CGL equations of state [30] with $p_{e\parallel} \propto n^3/B^2$ and $p_{e\perp} \propto nB$. The equations of state interpolate between theses two limits based on the portion of electrons that follow trapped trajectories.

III. RECONNECTION IN A FORCE-FREE SHEET

The first system that we study using the hybrid code with anisotropic electron equations of state is a force-free current sheet. This configuration, including the anisotropic electron equations of state, has previously been simulated using a two-fluid formulation in the HiFi numerical framework [25, 31]. A main conclusion of the fluid study was that including electron pressure anisotropy led to the formation of an extended electron current sheet in the exhaust, a feature observed in kinetic simulations but not captured in previous fluid codes. As described below, the hybrid model with electron anisotropy also reproduces the elongated current layer, while now also resolving ion kinetic effects.

It is relatively easy to implement the electron equations of state of Eqs. 2 and 3 in a force-free current sheet simulation because the initial density and magnetic field strength are uniform, and they therefore enter the equations of state only as global constants. In particular, the initial force-free current sheet in our simulations has magnetic field and density profiles of the form:

$$B_x(z) = B_0 \tanh(z/\lambda) \tag{4}$$

$$B_y(z) = \sqrt{B_g^2 + B_0^2 - B_x(z)^2} \tag{5}$$

$$B_z(z) = 0 \tag{6}$$

$$n(z) = n_0 \tag{7}$$

where we take $\lambda = 1 d_i = \sqrt{m_i c^2/\epsilon_0 n_0 e^2}$ and $B_g/B_0 = 0.3$. An initial magnetic perturbation of the form

$$\delta B_x(x,z) = -\delta B (L_x/2L_z) \cos(2\pi x/L_x) \sin(\pi z/L_z) \tag{8}$$

$$\delta B_z(x,z) = \delta B \sin(2\pi x/L_x) \cos(\pi z/L_z) \tag{9}$$

with $\delta B/B_0 = 0.01$ seeds reconnection with a single X-line. We initialize kinetic particle populations with Maxwellian distributions. In the fully kinetic simulation, the electron

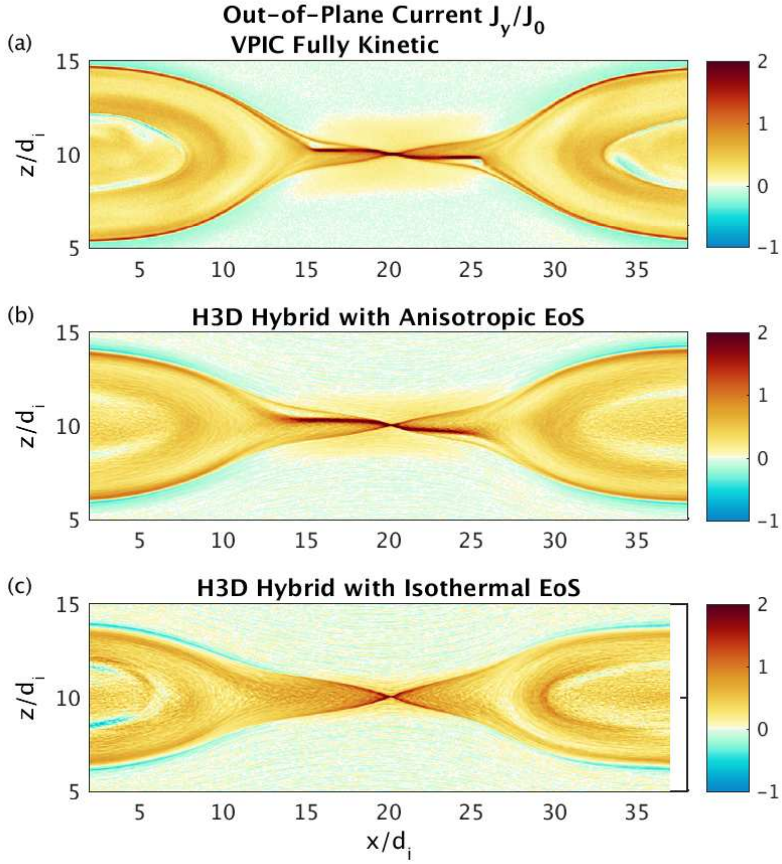

FIG. 1: Electron currents in a reconnected force-free sheet. The out-of-plane current density at time $t = 60/\Omega_{ci}$ from (a) a fully kinetic simulation, (b) a hybrid simulation with electron pressure anisotropy, and (c) a hybrid simulation with isotropic pressure.

Maxwellian is drifting in order to carry the parallel current that generates the sheared magnetic field. The initial uniform temperatures are chosen so that $\beta_e = 2\mu_0 n_0 T_e/B_0^2 = 0.1$ and $T_i/T_e = 5$. Simulations are performed in domains of size $L_x \times L_z = 40d_i \times 20d_i$ with 5120×2560 cells for the fully kinetic runs and 1024×1024 cells for the hybrid runs. The x boundaries are periodic, and the z boundaries are conducting and reflect particles. There are ~ 400 particles per cell of each kinetic species, and the fully kinetic runs had a mass ratio $m_i/m_e = 400$ and $\omega_{pe}/\Omega_{ce} = 2$.

The simulation parameters were selected so that the reconnection layer would fall into Regime 3 of Ref. [26]. This regime contains a moderate guide magnetic field that is strong enough to magnetize the electrons essentially everywhere, and the electron pressure remains anisotropic into the reconnection exhaust. An extended current layer may then form, which

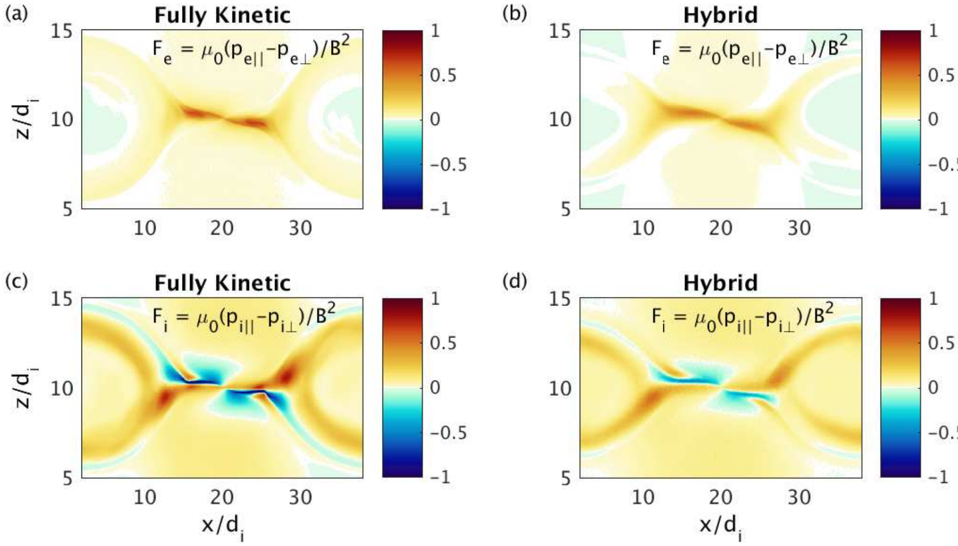

FIG. 2: Normalized pressure anisotropy measures $F = \mu_0(p_\parallel - p_\perp)/B^2$ ($F = 1$ is the firehose instability threshold). Electron anisotropy from (a) a fully kinetic simulation and (b) a hybrid simulation with anisotropic electron equations of state. The ion pressure is also anisotropic in both (c) the fully kinetic run and (d) the hybrid run.

is not limited to electron kinetic scales. As in the two-fluid simulations of Ref. [25], the most apparent difference between simulations with and without electron pressure anisotropy is the formation or absence of this extended electron current sheet. The out-of-plane current density is plotted in Fig. 1 from each of the three simulations. The extended exhaust current sheet that forms in the fully kinetic simulation in Fig. 1(a) is reproduced by the hybrid run with electron anisotropy in Fig. 1(b), while it does not appear in the hybrid simulation with isotropic, isothermal electrons in Fig. 1(c).

As described previously, the extended current sheets form when the electrons approach the firehose instability threshold $\mu_0(p_{e\parallel} - p_{e\perp})/B^2 \sim 1$ [25–27, 32, 33]. The normalized electron pressure measure $F_e = \mu_0(p_{e\parallel} - p_{e\perp})/B^2$ is plotted from the fully kinetic run in Fig. 2(a) and from the hybrid run with anisotropic closure in Fig. 2(b). In both cases, F_e peaks around 0.7. This level of pressure anisotropy is necessary to balance the $\mathbf{J} \times \mathbf{B}$ tension force on the electrons, and the anisotropy drives an additional cross-field electric current density $\mathbf{J_{e\perp}} \sim [(p_{e\parallel} - p_{e\perp})/B]\hat{\mathbf{b}} \times \hat{\mathbf{b}} \cdot \nabla\hat{\mathbf{b}}$. This regime thus requires a guide magnetic field strong enough the magnetize the electron orbits, but weak enough that the electron pressure anisotropy can balance the field line tension.

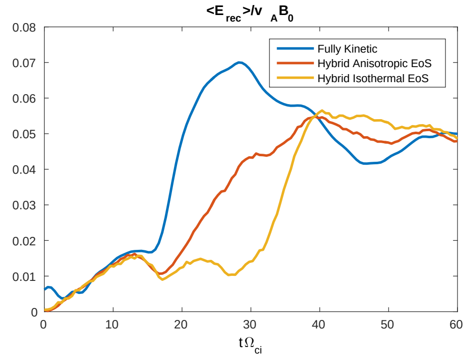

FIG. 3: The reconnection rate averaged over a $2d_i$ square box centered on the X-line. The saturated rates are similar in all cases.

Also plotted in Fig. 2 is the ion pressure anisotropy, which is captured by the kinetic treatment of the ions in the fully kinetic and hybrid formulations. In larger simulation domains, the ion pressure anisotropy is found to strongly influence the reconnection dynamics. It may, for example, be as important as ion inertia for setting the outflow speed of the reconnection exhaust [9]. And in addition to possibly driving instabilities, strong ion pressure anisotropy modifies the structure of boundary layers that may form in the exhaust [34]. The ions, however, are poorly magnetized in this regime with moderate guide field. As a result, the ion pressure is not only anisotropic in pitch angle with respect to the local magnetic field, but it is also anisotropic, or agyrotropic, with respect to the azimuthal direction around the magnetic field. The agyrotropy measure [35] applied to the ions $2(p_{i\perp 1} - p_{i\perp 2})/(p_{i\perp 1} + p_{i\perp 2}) > 0.3$ in large sections of the exhaust. It has been suggested that these ion kinetic effects are responsible for the discrepancy in the global evolution between kinetic (either hybrid or fully kinetic) models and Hall MHD models of reconnection during magnetic island coalescence [20].

The reconnection rates averaged over $2d_i$ boxes centered on the X-line are plotted over the course of the simulations in Fig. 3. During the initial transient phase, the reconnection rates differ. One reason is that secondary magnetic islands may form, and the details of this process are extremely sensitive to the initial conditions. In any case, the saturated reconnection rates are roughly the same for all three cases. The extended current sheet in the exhaust therefore does not in itself alter the quasi-steady reconnection rate.

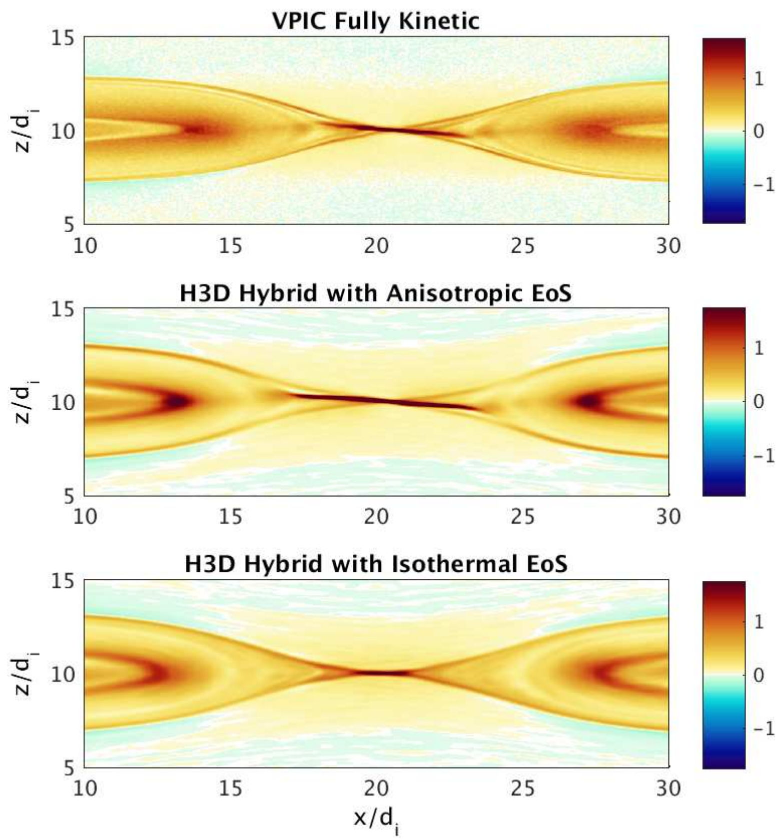

FIG. 4: Electron currents in a reconnected Harris sheet from (a) a fully kinetic simulation, (b) a hybrid simulation with electron pressure anisotropy, and (c) a hybrid simulation with isotropic pressure.

IV. RECONNECTION IN A HARRIS SHEET

The second system we consider is a reconnecting Harris sheet. The initial Harris sheet profiles are:

$$B_x(z) = B_0 \tanh(z/\lambda) \tag{10}$$

$$B_y(z) = B_g \tag{11}$$

$$B_z(z) = 0 \tag{12}$$

$$n(z) = n_b + n_0 \operatorname{sech}^2(z/\lambda) \tag{13}$$

where for our case we take $\lambda = 1 d_i$ and $B_g/B_0 = 0.2$. The initial temperatures are chosen with $T_i/T_e = 5$, while force balance across the layer now requires $n_0(T_i + T_e) = B_0^2/2\mu_0$. The background density is selected so $\beta_{e\infty} = 2\mu_0 n_b T_e / B_0^2 = 0.1$. The simulation domains are the same as for the force-free sheet; they are of size $L_x \times L_z = 40d_i \times 20d_i$ with 5120×2560 cells for the fully kinetic runs and 1024×1024 cells for the hybrid runs with periodic x boundaries and conducting z boundaries that reflect particles. There are again ~ 400 particles per cell of each kinetic species, and the fully kinetic runs had a mass ratio $m_i/m_e = 400$ and $\omega_{pe}/\Omega_{ce} = 2$.

The Harris sheet involves an additional complication to implement the anisotropic equations of state because the initial conditions no longer contain uniform magnetic field magnitude and density. The equations of state in Eqs. 2 and 3 involve quantities normalized to their upstream values, and the upstream values must now be determined independently for each flux tube. The initial upstream conditions must then be tracked for each flux tube as it convects, distorts, and possibly reconnects. In a 2D system, this is made possible by labeling each flux tube with a flux coordinate (out-of-plane vector potential component) Ψ. For the initial Harris sheet, Ψ is given by

$$\Psi = -B_0 \lambda \cdot \ln[\cosh(z/\lambda)], \tag{14}$$

and its time evolution follows from $\partial\Psi/\partial t = -E_y$. The initial Harris sheet density and magnetic field strength profiles may be written in terms of Ψ as:

$$n(\Psi) = n_b + n_0 \exp\left(\frac{2\Psi}{B_0\lambda}\right) \tag{15}$$

$$B(\Psi) = \sqrt{B_g^2 + B_0^2 - B_0^2 \exp\left(\frac{2\Psi}{B_0\lambda}\right)} \tag{16}$$

As the Harris sheet reconnects and $\Psi(x, z, t)$ evolves, the above expressions determine the initial upstream density and magnetic field at any point.

It turns out, however, that the values of n and B given by Eqs. 15 and 16 are not appropriate to use directly in the equations of state for the upstream normalizing factors n_∞ and B_∞. In particular, if Eqs. 15 and 16 were used as is, an unphysical pressure anisotropy would develop in the center of the Harris sheet when a perturbation of the form of Eq. 9 is included to seed reconnection. Additionally, in fully kinetic simulations, strong anistropy is not observed in the very center of the initial Harris sheet even later in the evolution. The anisotropy is typically most important once upstream plasma convects into the reconnection layer. In order to prevent this unphysical anisotropy from developing in the center of the

Harris sheet, we use the following technique. For the normalizing factor B_∞ that enters the equations of state, we use $B(\Psi)$ as in Eq. 16. On the other hand, for the density normalizing factor n_∞, we add an extra term δn to Eq. 15, so that $n_\infty = n(\Psi) + \delta n(\Psi)$. The term δn may be any function strongly peaked at the center of the initial Harris sheet, and we choose the particular function

$$\delta n(\Psi) = 5 \exp\left[-\left(\frac{2\Psi}{B_0\lambda}\right)^2 - 2(\tilde{B}^2 - 1)\right]. \tag{17}$$

Note that δn does not alter the physical density profile. It enters only in the normalization parameter n_∞ in the equations of state given by Eqs. 2 and 3. By making δn large in the center of the Harris sheet, the parameter α in the equations of state is made small, and the electrons remain in the isothermal limit in this region.

As in the case of the force-free sheet, electron pressure anisotropy allows an extended current sheet to form near the X-line. The out-of-plane current from each run is plotted in Fig. 4. Note that the current sheet is somewhat shorter in the fully kinetic run in Fig. 4(a) than the hybrid run with anisotropy in Fig. 4(b). This is in part because of the reduced mass ratio $m_i/m_e = 400$, which renders the electrons only marginally magnetized in the fully kinetic run. In particular, the parameter $K = \sqrt{R_B/\rho_e}$ (where R_B is the magnetic field line radius of curvature and ρ_e is the thermal electron Larmor radius) [36] dips to around 2.5 within the current sheet. This is the approximate cutoff for the electrons to be treated as fully magnetized, and the higher energy electrons do not have the adiabatic moment μ well-conserved if they cross the current sheet. The result is to somewhat reduce the electron pressure anisotropy from the levels predicted by the equations of state. At the physical proton mass ratio of $m_i/m_e = 1836$ and moderate electron β_e, the electrons are found to be well-magnetized at the guide field of $B_g/B_0 = 0.2$ used in this simulation [26].

The electron current sheet is again supported by electron pressure anisotropy close to the firehose threshold [see Fig. 5], and the current sheet exists where the anisotropy measure $F_e \gtrsim 0.5$. The ion pressure also becomes anisotropic as plotted in Figs. 5(c) and (d). As in the case of the force-free sheet, the ions also display substantial pressure agyrotropy.

The electron currents that are driven near the X-line by pressure anisotropy modify the structure of the Hall magnetic fields. The Hall field component B_y is plotted from each simulation in Fig. 6. The general quadrupolar structure, which results from the Hall term in the Ohm's law that freezes the magnetic field into the electron flow, is similar in all

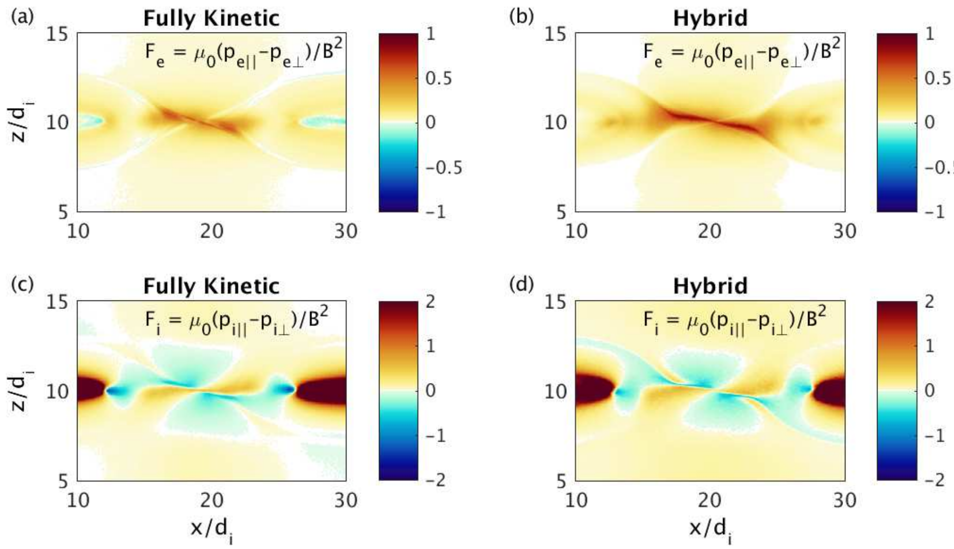

FIG. 5: Normalized pressure anisotropy measures $F = \mu_0(p_\parallel - p_\perp)/B^2$ for the Harris sheet. Electron anisotropy from (a) a fully kinetic simulation and (b) a hybrid simulation with anisotropic electron equations of state. The ion pressure anisotropy from (c) the fully kinetic run and (d) the hybrid run.

three cases. Nevertheless, the electron current sheet supported by anisotropy in the fully kinetic simulation and in the hybrid simulation with an anisotropic electron closure generates additional out-of-plane field near the X-line. This may be seen in the cuts along the mid-plane plotted in Fig. 6(d), where B_y is roughly 1.5-2 times as large at the X-line than its ambient value of $B_y/B_g = 0.2$ when there is electron pressure anisotropy, while it remains at approximately the background value for an isothermal electron closure. The anisotropic hybrid model does not agree precisely with the fully kinetic model both because the length of the electron current sheet is somewhat different in the two cases and because the residual electron pressure anisotropy in the exhaust is a little stronger in the hybrid run than in the fully kinetic run. As noted in Ref. [33], the magnetic field generated by the current sheet tempers the electron anisotropy (recall that the equations of state depend on B, and larger magnetic fields generate weaker anisotropy), so that the level of anisotropy saturates near the firehose threshold.

As seen in Fig. 7, the reconnection rate again reaches roughly the same level in all three models. Recently, it was shown that the double-adiabatic anisotropic CGL [30] electron equations of state allowed fast reconnection to occur in two-fluid simulations without the

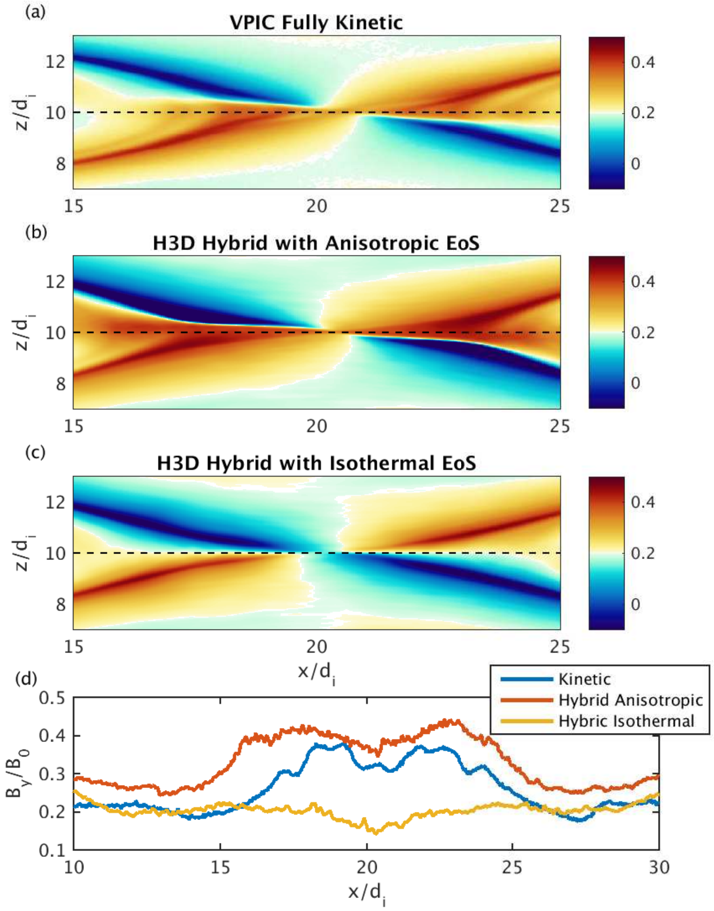

FIG. 6: Out-of-plane Hall magnetic field B_y profile generated during the reconnection of a Harris sheet in (a) the fully kinetic simulation, (b) the hybrid simulation with electron anisotropy, and (c) the hybrid simulation with isothermal electrons. (d) Cuts through the mid-plane reveal that currents driven by electron pressure anisotropy tend to increase the magnetic field strength near the X-line.

Hall effect [37]. The equations of state in Eqs. 2 and 3 do not lead to fast reconnection in themselves, however, and we find in the regime considered here that the electron anisotropy has little effect on the reconnection rate.

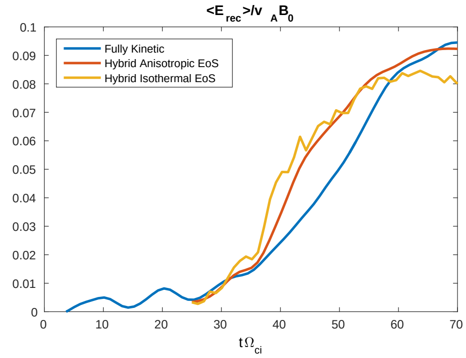

FIG. 7: Harris sheet reconnection rate. The reconnection rate averaged over a $2d_i$ square box centered on the X-line. Note that the hybrid simulations used a larger initial perturbation, and the simulations were aligned in time based on total initial reconnected flux.

V. SUMMARY

The equations of state for the electrons during reconnection with a guide field have been implemented in the hybrid code H3D. The equations of state account for electron pressure anisotropy that develops during reconnection and is caused by the adiabatic trapping of electrons. Simulations were performed of reconnection beginning from a force-free current sheet and from a Harris sheet with a moderate guide magnetic field. In both cases, extended current sheets formed centered on the X-line supported by electron pressure anisotropy with $\mu_0(p_{e\|} - p_{e\perp})/B^2 > 0.5$ in both the fully kinetic code and the hybrid code with an anisotropic electron closure. The electron current sheets remained very short in simulations that used an isothermal electron closure.

The hybrid code with anisotropic electron equations of state is therefore a first step towards the ability to simulate reconnection with moderate guide fields in large systems, such as global magnetosphere models, that nevertheless couple to ion kinetic length scales and where electron pressure anisotropy strongly modifies the magnetic structure of the reconnection layer. In 3D systems, the electron current sheets may be unstable and break apart into flux ropes [38], which could play a role in the formation of FTEs at the magnetopause. Before our model can be applied to more complex systems such the as the magnetosphere, however, important open questions must be solved. These questions include how to treat electron anisotropy and agyrotropy at reconnection sites with negligible guide magnetic fields and how to incorporate non-local effects into the electron closure in realistic 3D geometries with complicated initial conditions and without well-defined global flux surfaces.

Acknowledgments

A.L. received support from the LDRD office at LANL. W.D.'s work was supported by NASA's Heliophysics Theory Program. J.E. acknowledges support through NSF GEM award 1405166 and NASA grant NNX14AC68G. Simulations were performed on Pleiades provided by NASA's HEC Program, with LANL Institutional Computing resources, and on Mira provided by the ALCF at ANL.

---

[1] E. R. Priest and T. G. Forbes, Astronomy and Astrophysics Review **10**, 313 (2002), ISSN 0935-4956.

[2] T. Moore, J. Burch, W. Daughton, S. Fuselier, H. Hasegawa, S. Petrinec, and Z. Pu, Journal of Atmospheric and Solar-Terrestrial Physics **99**, 32 (2013).

[3] J. Birn, J. F. Drake, M. A. Shay, B. N. Rogers, R. E. Denton, M. Hesse, M. Kuznetsova, Z. W. Ma, A. Bhattacharjee, A. Otto, et al., J. Geophys. Res. **106**, 3715 (2001), ISSN 0148-0227.

[4] L. Wang, A. H. Hakim, A. Bhattacharjee, and K. Germaschewski, Physics of Plasmas (1994-present) **22**, 012108 (2015).

[5] M. M. Kuznetsova, M. Hesse, and D. Winske, Journal of Geophysical Research: Space Physics **105**, 7601 (2000), ISSN 2156-2202, URL `http://dx.doi.org/10.1029/1999JA900396`.

[6] J. Ng, Y.-M. Huang, A. Hakim, A. Bhattacharjee, A. Stanier, W. Daughton, L. Wang, and K. Germaschewski, Physics of Plasmas **22**, 112104 (2015), URL `http://scitation.aip.org/content/aip/journal/pop/22/11/10.1063/1.4935302`.

[7] J. U. Brackbill, Physics of Plasmas **18**, 032309 (2011), URL `http://scitation.aip.org/content/aip/journal/pop/18/3/10.1063/1.3568828`.

[8] S. Zenitani, I. Shinohara, T. Nagai, and T. Wada, Physics of Plasmas (1994-present) **20**, 092120 (2013), URL `http://scitation.aip.org/content/aip/journal/pop/20/9/10.1063/1.4821963`.

[9] A. Le, J. Egedal, J. Ng, H. Karimabadi, J. Scudder, V. Roytershteyn, W. Daughton, and Y.-H. Liu, Physics of Plasmas **21**, 012103 (2014), URL `http://scitation.aip.org/content/`

aip/journal/pop/21/1/10.1063/1.4861871.

[10] Y.-H. Liu, J. F. Drake, and M. Swisdak, Physics of Plasmas **18**, 062110 (pages 12) (2011), URL http://link.aip.org/link/?PHP/18/062110/1.

[11] D. Krauss-Varban and N. Omidi, Geophysical Research Letters **22**, 3271 (1995), ISSN 1944-8007, URL http://dx.doi.org/10.1029/95GL03414.

[12] Y. Lin and D. W. Swift, Journal of Geophysical Research: Space Physics (1978–2012) **101**, 19859 (1996).

[13] N. Aunai, M. Hesse, S. Zenitani, M. Kuznetsova, C. Black, R. Evans, and R. Smets, Physics of Plasmas (1994-present) **20**, 022902 (2013).

[14] R.-F. Lottermoser, M. Scholer, and A. P. Matthews, *Jour. Geophys. Res.* **103**, 4547 (1998).

[15] K. Arzner and M. Scholer, Journal of Geophysical Research: Space Physics (1978–2012) **106**, 3827 (2001).

[16] M. M. Kuznetsova, M. Hesse, and D. Winske, Journal of Geophysical Research: Space Physics (1978–2012) **106**, 3799 (2001).

[17] H. Karimabadi, V. Roytershteyn, H. X. Vu, Y. A. Omelchenko, J. Scudder, W. Daughton, A. Dimmock, K. Nykyri, M. Wan, D. Sibeck, et al., Physics of Plasmas **21**, 062308 (2014), URL http://scitation.aip.org/content/aip/journal/pop/21/6/10.1063/1.4882875.

[18] L. Yin, D. Winske, S. Gary, and J. Birn, Geophysical research letters **28**, 2173 (2001).

[19] L. Yin and D. Winske, Physics of Plasmas (1994-present) **10**, 1595 (2003).

[20] A. Stanier, W. Daughton, L. Chacón, H. Karimabadi, J. Ng, Y.-M. Huang, A. Hakim, and A. Bhattacharjee, Phys. Rev. Lett. **115**, 175004 (2015), URL http://link.aps.org/doi/10.1103/PhysRevLett.115.175004.

[21] A. Le, J. Egedal, W. Daughton, W. Fox, and N. Katz, Phys. Rev. Lett. **102**, 085001 (2009), ISSN 0031-9007.

[22] J. Egedal, W. Fox, N. Katz, M. Porkolab, M. Oieroset, R. P. Lin, W. Daughton, and J. F. Drake, J. Geophys. Res. **113**, A12207 (2008), ISSN A12207.

[23] J. Egedal, A. Le, and W. Daughton, Phys. Plasmas **20** (2013), ISSN 1070-664X.

[24] V. M. Vasyliunas, Reviews of Geophysics **13**, 303 (1975), ISSN 8755-1209.

[25] O. Ohia, J. Egedal, V. S. Lukin, W. Daughton, and A. Le, Phys. Rev. Lett. **109**, 115004 (2012), URL http://link.aps.org/doi/10.1103/PhysRevLett.109.115004.

[26] A. Le, J. Egedal, O. Ohia, W. Daughton, H. Karimabadi, and V. S. Lukin, Phys. Rev. Lett.

110, 135004 (2013), URL http://link.aps.org/doi/10.1103/PhysRevLett.110.135004.

[27] A. Le, J. Egedal, W. Daughton, J. F. Drake, W. Fox, and N. Katz, Geophys. Res. Lett. **37**, L03106 (2010), ISSN 0094-8276.

[28] M. Hesse, S. Zenitani, and A. Klimas, Phys. Plasmas **15**, 112102 (pages 5) (2008).

[29] L. J. Chen, N. Bessho, B. Lefebvre, H. Vaith, A. Fazakerley, A. Bhattacharjee, P. A. Puhl-Quinn, A. Runov, Y. Khotyaintsev, A. Vaivads, et al., J. Geophys. Res. **113** (2008), ISSN 0148-0227.

[30] G. F. Chew, M. L. Goldberger, and F. E. Low, Proc. Royal Soc. A **112**, 236 (1956).

[31] V. Lukin and M. Linton, Nonlinear Processes Geophys **18**, 871 (2011).

[32] S. W. H. Cowley, Planetary and Space Science **26**, 1037 (1978), ISSN 0032-0633.

[33] O. Ohia, J. Egedal, V. S. Lukin, W. Daughton, and A. Le, Geophysical Research Letters **42**, 10,549 (2015), ISSN 1944-8007, 2015GL067117, URL http://dx.doi.org/10.1002/2015GL067117.

[34] Y.-H. Liu, J. F. Drake, and M. Swisdak, Physics of Plasmas **18**, 092102 (pages 13) (2011), URL http://link.aip.org/link/?PHP/18/092102/1.

[35] J. Scudder and W. Daughton, Journal of Geophysical Research: Space Physics (1978–2012) **113** (2008).

[36] J. Buchner and L. Zelenyi, J. Geophys. Res. **94**, 11821 (1989).

[37] P. Cassak, R. Baylor, R. Fermo, M. Beidler, M. Shay, M. Swisdak, J. Drake, and H. Karimabadi, Physics of Plasmas (1994-present) **22**, 020705 (2015).

[38] W. Daughton, V. Roytershteyn, H. Karimabadi, L. Yin, B. J. Albright, B. Bergen, and K. J. Bowers, Nature Physics **7**, 539 (2011).